Theoretical approaches for hard electron bremsstrahlung and their scaling properties in the ultrarelativistic regime

D. H. Jakubassa-Amundsen
Mathematics Institute, University of Munich, Theresienstrasse 39, 80333 Munich, Germany

(Received 23 August 2021; revised 6 October 2021; accepted 18 October 2021; published 1 November 2021)

Bremsstrahlung angular and frequency distributions from 35-MeV electrons colliding with lead are calculated within the Dirac partial-wave (DW) theory. These benchmark results are compared with the Dirac-asymptotic Sommerfeld-Maue approach, with an analytical approximation to this DaSM model, and with the Sommerfeld-Maue (SM) theory, in order to investigate the validity of these simpler theories for photons with frequencies beyond 25 MeV. Scaling properties with respect to the collision energy, the photon emission angle, and the energy of the scattered electron are used to extend the predictions at 35 MeV to higher collision energies. For the angle-integrated photon spectrum a Green's-function-based theory by Milstein and coworkers [J. Exp. Theor. Phys. **100**, 1 (2005)] serves as a complement to the DW theory at the lower photon frequencies. Earlier conjectures are confirmed that, for the singly differential cross section, the SM theory is applicable for frequencies at least some 5 MeV below the short-wavelength limit.

DOI: 10.1103/PhysRevA.104.052802

I. INTRODUCTION

There has been a revived interest in high-energy electron bremsstrahlung, both experimentally [1–3] and theoretically [4–7]. Its description is commonly performed within the Dirac partial-wave (DW) theory [8,9], where the continuum states of the scattering electron in a strong central potential are calculated with the help of the Dirac equation.

Since the feasibility of such accurate calculations is limited to collision energies up to some tens of MeV, there has been the long-standing question how to establish a bremsstrahlung theory, applicable at still higher energies, which is complementary to the DW theory and has a comparable accuracy.

In their seminal paper [10], Bethe and Maximon demonstrated that the Sommerfeld-Maue (SM) wave functions, analytically available for a pure Coulomb field, are accurate approximations to the Dirac partial waves for electron energies at least of the order of 50 MeV, irrespective of the strength of the central potential. Hence, hybrid bremsstrahlung theories were developed. In the Dirac-Sommerfeld-Maue (DSM) model [11], the DW for the incoming electron is replaced by a SM function. This theory is feasible at ultrarelativistic energies but only at the short-wavelength limit (SWL). In order to cover lower photon frequencies within a manageable computation time, a high-energy approximation to the initial-state SM function was introduced, leading to the Dirac-asymptotic Sommerfeld-Maue (DaSM) theory [12] or to an analytical approximation to it [13,14].

The Sommerfeld-Maue prescription [10,15], an analytical bremsstrahlung theory where also the outgoing electron is represented by a SM function, is for heavy targets only applicable if the scattered electron is sufficiently energetic. In fact, it was recently shown that the singly differential bremsstrahlung spectrum, measured for 500-MeV electrons colliding with targets up to gold and covering photon frequencies extending to 250 MeV, can well be described within the SM theory [3].

It is the motivation of the present work to bridge the gap between the DSM, respectively DaSM, approaches for photons near the upper end of the spectrum and the SM theory for the softer photons. To this aim, a collision energy of 35 MeV is chosen which is sufficiently high so that the initial-state SM function becomes accurate, but low enough to make DW calculations feasible. This enables us to establish, by means of a comparison with the DW theory, the validity of the DSM and the DaSM approaches for fixed photon frequencies and emission angles. These results are then set against the SM theory in order to estimate the largest possible frequency for which this theory is applicable.

The transfer of these results to collision energies beyond 35 MeV is made possible by the existence of scaling laws for the bremsstrahlung intensity. It was discovered by Jabbur and Pratt [16] that the singly differential cross section at the SWL scales with the inverse collision energy. Recently it was found that also the doubly differential cross section close to the SWL scales with the collision energy, provided the photon emission angle is scaled accordingly [12]. It will be shown that the photon angular distribution even scales with the energy of the slow outgoing electron for not too large angles.

The paper is organized as follows. Section II provides a short overview over the theoretical approaches. Numerical results are presented in Sec. III for the doubly differential and the singly differential bremsstrahlung cross sections, including an investigation of the validity of the scaling laws within the various models. The polarization transfer from a spin-polarized electron to the photon is also briefly referred to. The conclusion is given in Sec. IV. Atomic units ($\hbar = m = e = 1$) are used unless indicated otherwise.

II. THEORETICAL MODELS

We consider bremsstrahlung from relativistic electrons colliding with atoms and restrict ourselves in this section to the experimental situation of unpolarized particles. The doubly differential cross section for the emission of a photon with frequency ω into the solid angle $d\Omega_k$ is given by

$$\frac{d^2\sigma}{d\omega d\Omega_k} = \frac{4\pi^2\omega\, k_f E_i E_f}{c^5\, k_i}\,\frac{1}{2}\sum_{\sigma_i,\sigma_f}\sum_{\lambda}\int d\Omega_f |W_{\text{rad}}(\sigma_f,\sigma_i)|^2, \tag{2.1}$$

where $\boldsymbol{k}_i, E_i$ and $\boldsymbol{k}_f, E_f$ are, respectively, the momentum and total energy of the incoming and scattered electrons, and the integration is over the final direction of the electron. W_{rad} is the radiation matrix element,

$$W_{\text{rad}}(\sigma_f,\sigma_i) = \int d\boldsymbol{r}\, \psi_f^{(\sigma_f)+}(\boldsymbol{r})(\boldsymbol{\alpha}\boldsymbol{\epsilon}_\lambda^*)e^{-i\boldsymbol{k}\boldsymbol{r}}\psi_i^{(\sigma_i)}(\boldsymbol{r}). \tag{2.2}$$

The electronic states are described by the initial ($\psi_i^{(\sigma_i)}$) and final ($\psi_f^{(\sigma_f)}$) wave functions, and (2.1) includes an average over the initial spin projection (σ_i) and a sum over the final spin projection (σ_f). The photon is characterized by its momentum $\boldsymbol{k}$ and its polarization direction $\boldsymbol{\epsilon}_\lambda$, over which it is also summed. $\boldsymbol{\alpha}$ is a vector of Dirac matrices. A coordinate system is chosen where the z axis is taken along $\boldsymbol{k}_i$, the y axis along $\boldsymbol{k}_i \times \boldsymbol{k}$, and the x axis along $\boldsymbol{e}_y \times \boldsymbol{k}_i$.

We are considering fast collisions with the kinetic energy $E_{i,\text{kin}} = E_i - c^2 \geqslant 35$ MeV and mostly small photon emission angles ($\theta_k \lesssim 20°$), such that nuclear size effects are usually negligible. Moreover, we consider only hard photons in the upper third of the spectrum. Therefore, also screening effects by the atomic electrons are at most in the percent region [7]. This means that the potential between the scattering electron and the atom is well represented by a pure Coulomb field, $-Z/r$, with Z being the nuclear charge number.

The bremsstrahlung theories considered here differ only in the choice of the electronic wave functions. In the state-of-the-art prescription, the Dirac partial-wave theory [8], they are continuum solutions to the Dirac equation. Their partial-wave expansion renders the integration over $d\Omega_f$ trivial, such that, after carrying out the sum over σ_f, (2.1) reduces to

$$\frac{d^2\sigma^{\text{DW}}}{d\omega d\Omega_k} = \frac{2\pi^2\omega\, k_f E_i E_f}{c^5\, k_i}\sum_{\sigma_i,\lambda}\sum_{\kappa_f,m_f} \times \left|\int d\boldsymbol{r}\, \psi^+_{\kappa_f m_f}(\boldsymbol{r})(\boldsymbol{\alpha}\boldsymbol{\epsilon}_\lambda^*)e^{-i\boldsymbol{k}\boldsymbol{r}}\, \psi_i^{(\sigma_i)}(\boldsymbol{r})\right|^2, \tag{2.3}$$

where $\psi_{\kappa_f m_f}(\boldsymbol{r}) = \binom{g_{\kappa_f}(r)Y_{j_f l_f m_f}(\Omega)}{if_{\kappa_f}(r)Y_{j_f l'_f m_f}(\Omega)}$ is constructed from the large (g_{κ_f}) and small (f_{κ_f}) components of the radial Dirac partial wave. The angular part of $\psi_{\kappa_f m_f}$ is expressed in terms of a spherical harmonic spinor, $Y_{j_f l_f m_f}$ [17]. The angular momentum quantum numbers are denoted by κ_f and m_f, respectively, j_f, l_f, and m_f, interrelated by $l_f = |\kappa_f + \frac{1}{2}| - \frac{1}{2}$, $l'_f = |\kappa_f - \frac{1}{2}| - \frac{1}{2}$, and $j_f = |\kappa_f| - \frac{1}{2}$.

In the Dirac–Sommerfeld-Maue theory, $\psi_f^{(\sigma_f)}$ is the same as above. At the short-wavelength limit, this function has a simple representation in terms of Bessel functions [11,18]. On the other hand, the exact Dirac solution $\psi_i^{(\sigma_i)}$ is replaced by a SM wave function [10,15],

$$\psi_i^{\text{SM}(\sigma_i)}(\boldsymbol{r}) = \frac{e^{\pi\eta_i/2}}{(2\pi)^{3/2}}\Gamma(1-i\eta_i)e^{i\boldsymbol{k}_i\boldsymbol{r}} \times \left(1 - \frac{ic}{2E_i}\boldsymbol{\alpha}\nabla\right)\, {}_1F_1(i\eta_i, 1, i(k_i r - \boldsymbol{k}_i\boldsymbol{r}))\, u_{k_i}^{(\sigma_i)}, \tag{2.4}$$

where $\eta_i = \frac{ZE_i}{k_i c^2}$ is the Sommerfeld parameter, Γ is the Gamma function, ${}_1F_1$ is a confluent hypergeometric function, and $u_{k_i}^{(\sigma_i)}$ is a free 4-spinor.

The extension of the DSM model to lower frequencies is unfortunately not feasible because of excessively long computation times. However, for small photon angles, relating to a small momentum transfer and hence to large distances, an asymptotic representation of the ${}_1F_1$ function in (2.4) can be used [19], which results in the simple asymptotic form of ψ_i^{SM},

$$\psi_i^{\text{aSM}(\sigma_i)}(\boldsymbol{r}) = \frac{1}{(2\pi)^{3/2}}e^{i\boldsymbol{k}_i\boldsymbol{r}}(k_i r - \boldsymbol{k}_i\boldsymbol{r})^{-i\eta_i}u_{k_i}^{(\sigma_i)}. \tag{2.5}$$

The use of (2.5) together with an exact Coulombic final-state function leads to the DaSM theory [12]. The advantage of the closed expressions (2.4) and (2.5) used, respectively, in the DSM and DaSM theories, consists in allowing bremsstrahlung estimates at arbitrarily high collision energies. This has to be contrasted to the exact DW prescription where the required number of initial partial waves and hence the computation time increases strongly with E_i.

The Di Piazza-Milstein (PM) approach to the DaSM theory [14], while using the asymptotic representation (2.5) for the initial state, introduces additional approximations into the final state. They are based on the fact that for small photon emission angles θ_k, the main contribution to the sum over m_f in (2.3) is due to the terms with $m_f = \pm\frac{1}{2}$, such that only those are kept. In consistency with this restriction, and implying that also the angle θ between $\boldsymbol{k}_i$ and $\boldsymbol{r}$ is small, any angular dependence of $\psi_{\kappa_f m_f}(\boldsymbol{r})$ is neglected. Hence, $Y_{j_f l_f m_f}$ is approximated by

$$Y_{j_f l_f m_f}(\Omega) \approx \sqrt{\frac{2l_f+1}{4\pi}}\left(l_f 0 \frac{1}{2}\, m_f | j_f m_f\right)\chi_{m_f}, \tag{2.6}$$

with $\chi_{\frac{1}{2}} = \binom{1}{0}$ and $\chi_{-\frac{1}{2}} = \binom{0}{1}$ and where $(l_f 0 \frac{1}{2} m_f | j_f m_f)$ is a Clebsch-Gordan coefficient.

In order to arrive at an analytical expression for the radiation matrix element, further approximations are made in the angular integral of (2.3), like replacing $\sin\theta$ by θ and replacing the upper integration limit π by infinity, such that

$$\int d\Omega\, e^{i(\boldsymbol{k}_i-\boldsymbol{k})\boldsymbol{r}}(1-\cos\theta)^{-i\eta_i} \approx e^{iE_f r/c}\, 2^{i\eta_i}\int_0^\pi \sin\theta\, d\theta\, \theta^{-2i\eta_i} \times 2\pi\, J_0(kr\theta\sin\theta_k) \approx e^{iE_f r/c}\frac{2^{2-i\eta_i}\pi\,\Gamma(1-i\eta_i)}{(kr\sin\theta_k)^{2-2i\eta_i}\Gamma(i\eta_i)}. \tag{2.7}$$

These approximations are, however, invalid at $\theta_k = 0$ where the Bessel function $J_0(0) = 1$, leading to a divergent integral. With the analytical representations of g_{κ_f} and f_{κ_f} for a pure

Coulomb field, the remaining radial integral exists in closed form. The Di Piazza–Milstein formula for the doubly differential bremsstrahlung cross section is given in the Appendix.

If the frequency of the emitted photon is sufficiently small such that the scattered electron remains ultrarelativistic, the exact final Dirac function in (2.2) can also be replaced by a Sommerfeld-Maue function. Then the radiation matrix element (2.2) with (2.4) exists in an analytical form [15]. Although the integration over the direction of the scattered electron has to be carried out numerically, the SM bremsstrahlung cross section is readily evaluated for arbitrary E_i and ω.

III. NUMERICAL RESULTS

Whereas a comparison between the DW, the DSM, and the SM approaches at the SWL was investigated earlier [7,11], we present here a systematic study, testing the validity not only of the DaSM and SM theories at lower photon frequencies but also of the Di Piazza–Milstein approximation, which we evaluate here for bremsstrahlung.

The reference DW calculation at 35 MeV was carried out with the help of the Fortran code RADIAL from Salvat *et al.* [20] for solving the Dirac equation for the initial and final electronic states. The radial integrals were performed numerically by means of the complex-plane rotation method (CRM), introduced by Yerokhin and Surzhykov into the bremsstrahlung theory [9]. Finite nuclear size effects within a Fourier-Bessel representation of the ^{208}Pb nuclear charge density [21] were considered in all DW results. However, even at $\theta_k = 21^\circ$, the highest angle investigated, the difference to the Coulombic result is only 2.5% near the SWL (decreasing with decreasing momentum transfer, i.e., with increasing E_f or decreasing θ_k). The necessary number of partial waves is related to the inverse of the minimum momentum transfer $q = |\boldsymbol{k}_i - \boldsymbol{k}_f - \boldsymbol{k}|$ [22], which determines the impact parameter and thus the maximum angular momentum $l_{\max}$ which is required for a given collision process. Near the SWL and at forward angles, $l_{\max} \sim k_i/q \approx k_i/|\boldsymbol{k}_i - \boldsymbol{k}| \approx 1/\theta_k$. On the other hand, limiting the impact parameter by the range of the atomic target potential, one gets $l_{\max} \sim k_i$ [10]. In our calculation, partial waves $|\kappa_i|$ up to 400–460 and $|\kappa_f|$ up to 40–45 were used (which still may lead to too low cross sections at the smallest angles considered). For a higher number of partial waves, the results get unstable. Numerical details can be found in Ref. [23].

A. Doubly differential cross section

Figure 1(a) shows the photon angular distribution at the tip of the spectrum. Comparison is made between the DSM results on one hand and the DaSM, PM, and SM results on the other hand. From previous work [7] it is known that the DSM is validated by the close agreement with formally screened DW results for collision energies above 25 MeV. While the DSM is evaluated at the tip (more precisely, at a tiny final kinetic energy, $E_{f,\mathrm{kin}} = 10$ eV), numerical inaccuracies prevent the DaSM from being stable too close to the tip; therefore, $E_{f,\mathrm{kin}} = 3$ keV was taken for the other three theories. This introduces an error of about 2% at 0°, decreasing with the angle (1% at 0.5°, 0.2% at 3°). While the SM theory fails at the SWL, the DaSM coincides with the DSM up to $\theta_k \sim 2^\circ$.

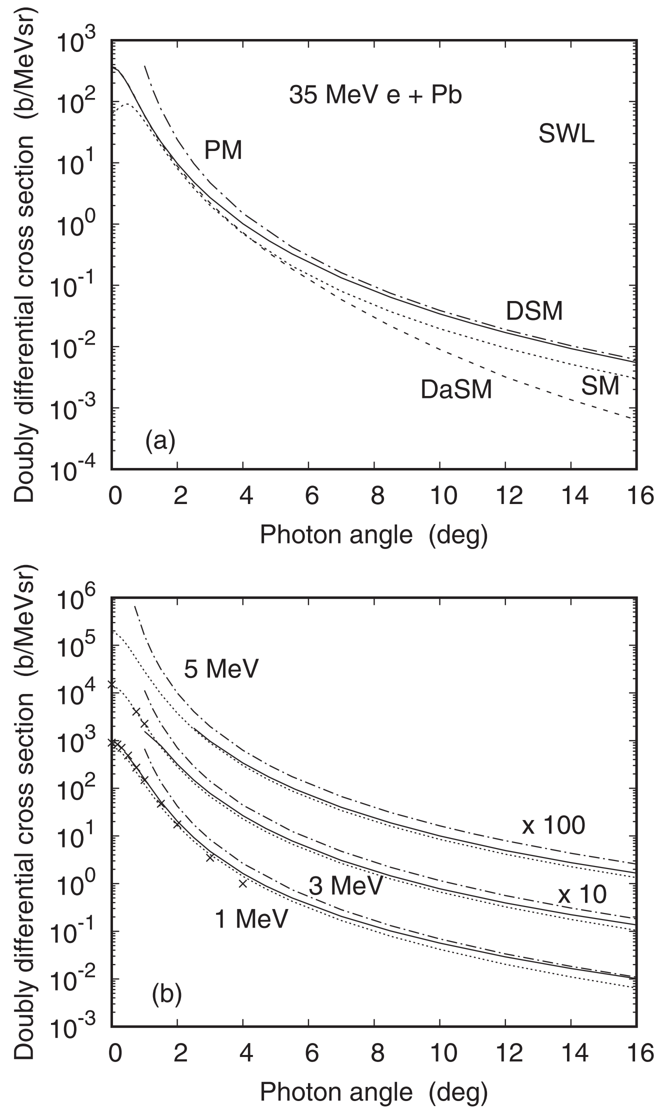

FIG. 1. (a) Doubly differential bremsstrahlung cross section $\frac{d^2\sigma}{d\omega d\Omega_k}$ from 35-MeV electrons colliding with ^{208}Pb as a function of the photon angle θ_k at the SWL. Shown are results from the DSM (———), the DaSM (– – – –), the SM (· · · · · ·), and the PM (– · –) approaches. (b) $\frac{d^2\sigma}{d\omega d\Omega_k}$ at $E_{f,\mathrm{kin}} = 1$ MeV (lower curves), 3 MeV (middle curves, all multiplied by a factor of 10), and 5 MeV (uppermost curves, multiplied by 100 for better visibility). Shown are results from the DW (———), DaSM (× × ×), SM (· · · · · ·), and PM (– · –) approaches.

The PM results clearly show the divergence for $\theta_k \to 0$, but they get very close to the DSM results for $\theta_k \gtrsim 10^\circ$.

The respective comparison for final kinetic energies between 1 and 5 MeV is displayed in Fig. 1(b). Since $\omega = E_i - E_f$, they correspond to photon frequencies of 34, 32, and 30 MeV. The requirement of a manageable number of partial waves allows DW results only beyond 0.5°, 1°, and 2.5° for $E_{f,\mathrm{kin}} = 1$, 3, and 5 MeV, respectively.

Since the DaSM omits initial partial waves, the efficient CRM is not applicable because the separation of radial and angular integrals is no longer possible. Instead, a convergence inducing factor $e^{-\epsilon r}$ is required for the occurring double integrals [12]. For small angles and high final energies, ϵ has

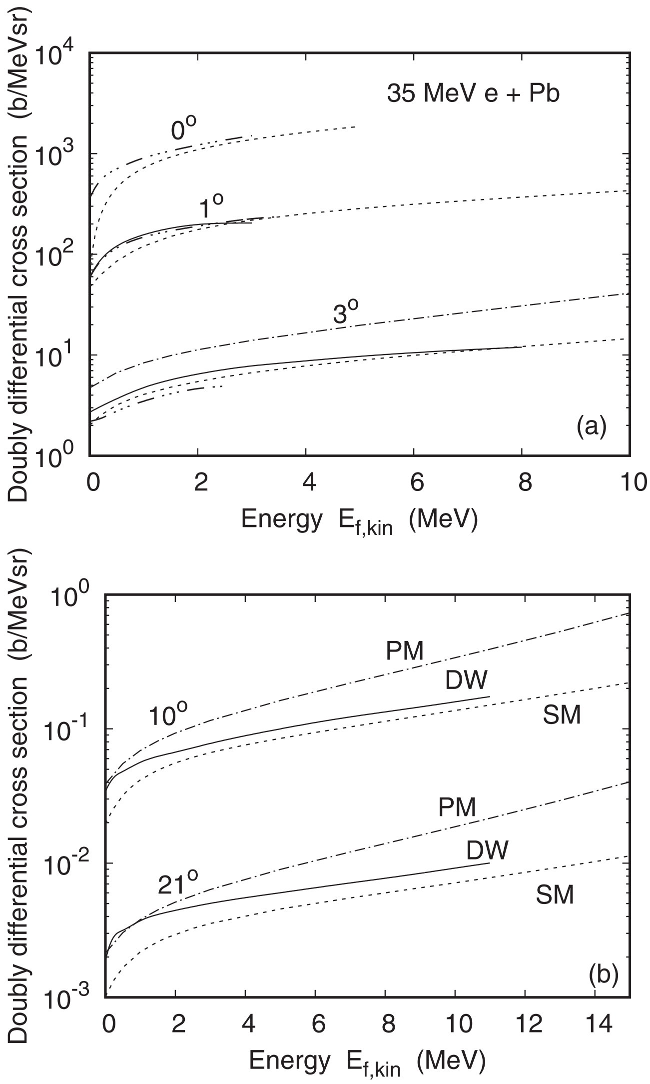

FIG. 2. Doubly differential bremsstrahlung cross section from 35-MeV $e + {}^{208}$Pb collisions as a function of the final electron energy $E_{f,\mathrm{kin}}$ at (a) photon angles θ_k of 0° (uppermost curves), 1° (middle curves), and 3° (lower curves) and (b) photon angles θ_k of 10° (upper curves) and 21° (lower curves). Shown are results from the DWi (——), DaSM (— · · · —), SM (— — ——), and PM (— · —) approaches.

to be taken particularly small, implying a large integration interval over a strongly oscillating function. This results in computation times of several weeks on a conventional work station for just one cross-section value. (Indeed, for the more complicated DSM theory, if extended to nonzero k_f, the computation time would be considerably higher since the same evaluation method is used.) Hence, DaSM results are only provided for $E_{f,\mathrm{kin}} \leqslant 3.5$ MeV. However, these DaSM results cover the angular region $\theta_k \lesssim 1°$ where the DW calculations for higher E_f are hampered by the lack of convergence. Given the fact that the DaSM agrees with the DW for angles between 0.5° and 1° at $E_{f,\mathrm{kin}} \leqslant 2$ MeV (Fig. 1), the DaSM results can be considered complementary to the DW results for all angles up to 1°. At the larger angles it is seen that the SM results get closer to the DW ones with increasing E_f, whereas the PM results show the opposite trend.

Profiting from the coincidence of the DaSM and the DW results near 1°, we define a merged theory, termed DWm, which refers to the use of the DaSM at $\theta_k \leqslant 0.5°$–$0.7°$ and of the DW for $\theta_k \geqslant 0.75°$–$1°$. In a similar fashion we introduce an interpolated theory, termed DWi, which uses the DSM grid point at $E_{f,\mathrm{kin}} \approx 0$ and the DW grid points for $E_{f,\mathrm{kin}} \geqslant 0.2$ MeV where the partial-wave expansion is numerically stable and well converged.

Figure 2 compares the photon spectrum (respectively the dependence on $E_{f,\mathrm{kin}}$) at fixed photon angles between 0° and 21° as obtained from the different bremsstrahlung theories. Emphasis is again put on the approach of the SM results towards the DaSM (at 0°), respectively DW results (at $\theta_k \geqslant 1°$) with decreasing photon frequency (respectively, increasing energy of the scattered electron). It is seen that this convergence occurs at higher $E_{f,\mathrm{kin}}$ the larger the angle. The crossing of the DW and SM curves for $\theta_k = 1°$ near $E_{f,\mathrm{kin}} = 2.5$ MeV [Fig. 2(a)] is spurious and due to the lack of convergence of the DW calculations (resulting in too low cross-section predictions). In concord with Fig. 1(a), there is agreement between the DW and the DaSM results at $\theta_k = 1°$, while the DaSM theory underpredicts the cross section at the higher angles. The PM approximation is reliable for angles near and beyond 10°, but only in the vicinity of the SWL. Its increase with $E_{f,\mathrm{kin}}$ is considerably steeper than predicted by the DW prescription.

B. Scaling laws

When comparing angular bremsstrahlung distributions at different collision energies, it was observed that there is a linear increase of intensity, and a corresponding decrease of the photon angle, with the ratio of the higher to the lower impact energy. This behavior can be quantified according to [12].[1]

$$\frac{d^2\sigma}{d\omega d\Omega_k}\big(E_{i,\mathrm{kin}}^{(1)},\theta_k\big) \approx \frac{E_{i,\mathrm{kin}}^{(1)}}{E_{i,\mathrm{kin}}^{(2)}}\frac{d^2\sigma}{d\omega d\Omega_k}\left(E_{i,\mathrm{kin}}^{(2)},\frac{E_{i,\mathrm{kin}}^{(1)}}{E_{i,\mathrm{kin}}^{(2)}}\,\theta_k\right). \tag{3.1}$$

In Fig. 3 this scaling is investigated at the SWL and at 3 MeV, using collision energies of 35, 100, and 500 MeV. Referring to the pair 35 MeV/100 MeV at the SWL, shown in Fig. 3(a) (the angular scale on the figure corresponds to the 100-MeV impact), the SM theory obeys the scaling (on the percent level) up to angles near 1°, whereas for the DSM and the PM prescriptions the scaling holds for angles $\lesssim 3°$. At 3 MeV, the SM theory scales up to 18° (except for the smallest angles), but the PM theory does not. However, the scaling generally improves with collision energy, and the PM results get closer to the SM ones. In fact, at 500-MeV impact the PM angular dependence is nearly the same as predicted by the SM theory for $\theta_k \gtrsim 6°$ [Fig. 3(b)]. Also shown for $E_{f,\mathrm{kin}} = 3$ MeV are the merged results from the DWm, scaled to $E_{i,\mathrm{kin}} = 100$ MeV and hence extending only to $\theta_k = 5.6°$. Their close agreement with the other models beyond 1° indicates that the scaling should also hold for the DW theory up to 3 MeV.

[1] In Ref. [12] the following typos occurred: In (4.1) and (4.7), $100\,\theta_k/E_{i,\mathrm{kin}}$ should read $E_{i,\mathrm{kin}}\theta_k/100$, and two lines above (4.7), $E_{i,\mathrm{kin}}/100$ MeV $\times\,\theta_k$ should be replaced by 100 MeV$/E_{i,\mathrm{kin}} \times \theta_k$.

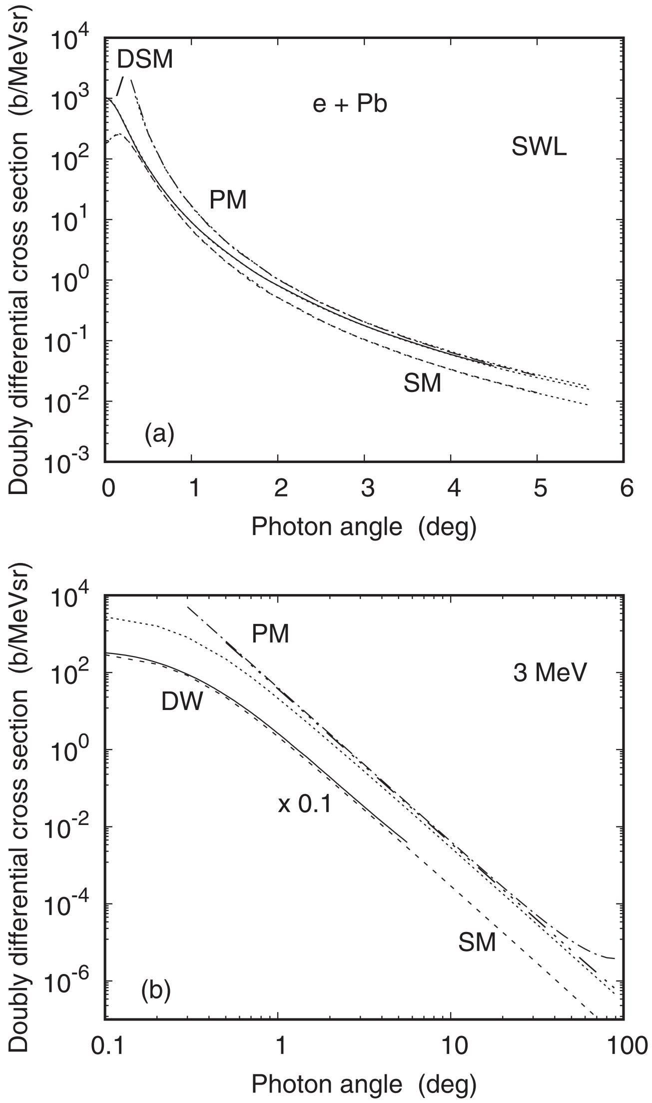

FIG. 3. (a) Doubly differential bremsstrahlung cross section from $e + {}^{208}$Pb collisions as a function of the photon angle θ_k at the SWL. Shown at $E_{i,\rm kin} = 100$ MeV are results from the DSM (——, $E_{f,\rm kin} = 30$ eV), SM (— — ——, $E_{f,\rm kin} = 3$ keV), and PM (— · —, $E_{f,\rm kin} = 3$ keV) approaches. Included are the respective scaled results from 35-MeV impact (······), obtained from (3.1) with $E_{i,\rm kin}^{(1)} = 100$ MeV and $E_{i,\rm kin}^{(2)} = 35$ MeV. These results are explicitly shown beyond 5°, while coinciding in the plot with the respective 100-MeV results elsewhere. (b) $\frac{d^2\sigma}{d\omega d\Omega_k}$ for $E_{f,\rm kin} = 3$ MeV. Shown are the PM results at $E_{i,\rm kin} = 100$ MeV (— · —), and at $E_{i,\rm kin} = 500$ MeV the scaled SM (······) and PM (— ··· —) results are shown. Included (but multiplied by a factor of 0.1 for better visibility) are the SM results at $E_{i,\rm kin} = 100$ MeV (— — ——) and the scaled merged DWm results at $E_{i,\rm kin} = 35$ MeV. (The 100-MeV and the scaled 500-MeV SM curves would coincide up to $\theta_k = 50°$ if the former were not shifted down.)

Figure 4 provides a comparison of the photon angular dependence for 35-MeV collision energy for various photon frequencies, respectively final electron energies. The results for $E_{f,\rm kin}$ at and below 2 MeV were obtained from the merged DWm prescription. Profiting from the fact that for $E_{f,\rm kin} \leqslant 2$ MeV the curves coincide up to $\theta_k \approx 5°$ (by means of multiplication with appropriate global factors), this scaling with $E_{f,\rm kin}$ was applied to create for $E_{f,\rm kin} = 3$ MeV additional DaSM grid points below 0.75°. At 5 MeV, results (from DW) are only shown beyond 2.5°. In the interval 1 MeV $\leqslant E_{f,\rm kin} \leqslant 5$ MeV, the doubly differential cross section decreases with $E_{f,\rm kin}$ on the average like $E_{f,\rm kin}^{-0.45}$, getting slightly steeper with increasing final energy.

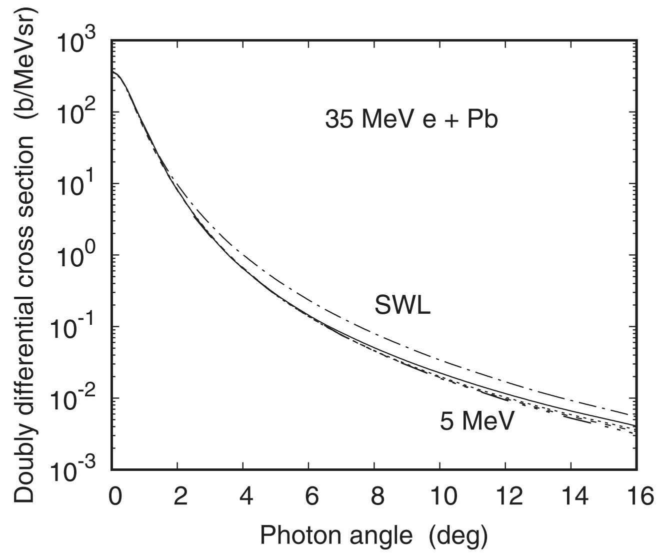

FIG. 4. Final-energy-scaled doubly differential bremsstrahlung cross section from 35-MeV $e + {}^{208}$Pb collisions as a function of the photon angle θ_k. Shown is the DSM result at the SWL (— · —), as well as the merged DWm results at $E_{f,\rm kin} = 1$ MeV (multiplied by a factor of 0.4, ——), 2 MeV (multiplied by 0.3, ······), and 3 MeV (multiplied by 0.25, — — ——). Also shown is the DW result at 5 MeV (multiplied by 0.19, — ··· —). All curves are fitted to the DSM result at the small angles and approach the DW result with increasing final energy.

Figure 5 displays the scaled results for a fixed photon angle as function of the photon frequency, respectively of the energy of the scattered electron. For the collision energy of 100 MeV, the selected angles are $\theta_k = 0°$, 0.35°, 1.05°, and 3.5°. The displayed results for 35 MeV, which are multiplied by the scaling factor $\frac{100}{35}$, are obtained from using the scaled angles $\frac{100}{35}\theta_k = 0°, 1°, 3°$, and 10°.

For the smallest angles [Fig. 5(a)], the DaSM approach as well as the SM theory obey the scaling up to $E_{f,\rm kin} \approx 2$ MeV, but only on the 5% level. For the larger angles [Fig. 5(b)], results from the DW theory and from the PM model are shown in addition. While the scaled DaSM theory at 35-MeV collision energy (and $\theta_k = 3°$) underpredicts the respective DW estimates, it gradually approaches these DW estimates when the impact energy is increased to 100 MeV and further to 500 MeV (for the highest energy, $\theta_k = 0.21°$ has to be used). This is in concord with the earlier result that also for the DaSM theory scaling improves with collision energy at fixed E_f for the larger angles [12].

For the highest angle (10° at 35 MeV), Fig. 5(c), the approach of the PM model to the DW theory is demonstrated when the collision energy is increased from 35 to 500 MeV. In the lower part of this figure, the respective SM results are

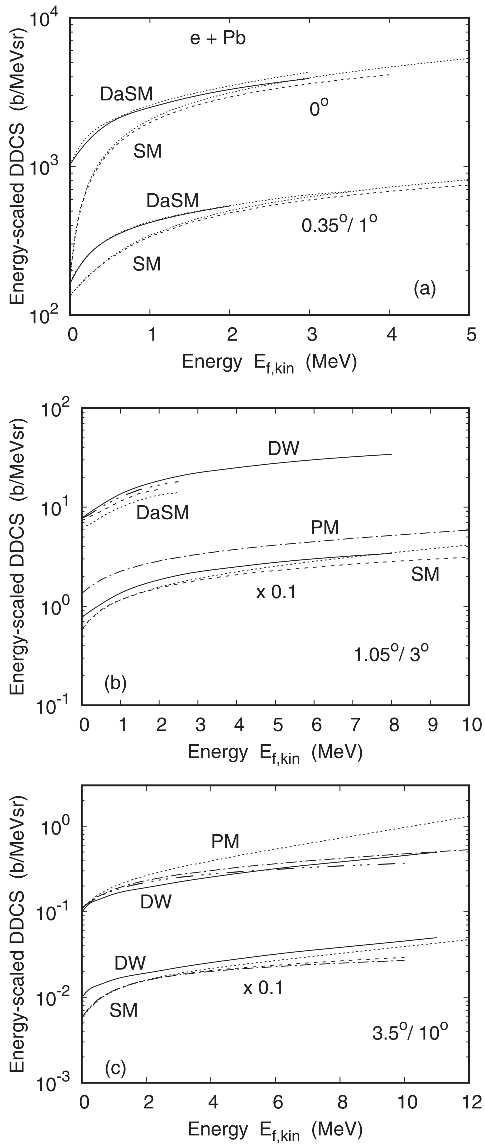

FIG. 5. (a) Collision-energy-scaled doubly differential bremsstrahlung cross section from electron impact on ^{208}Pb as a function of the energy $E_{f,\rm kin}$ of the scattered electron. Shown for 100 MeV impact and angles 0° (top curves) and 0.35° (bottom curves) are results from the DaSM (——) and SM (− − −−) theories, as well as the respective scaled results from the 35-MeV impact (······) at angles 0° (top curves) and 1° (bottom curves). (b) $\frac{d^2\sigma}{d\omega d\Omega_k}$ at $E_{i,\rm kin} = 100$ MeV and $\theta_k = 1.05°$. The top curves show the DaSM results (− − −−) and the scaled DaSM results at $E_{i,\rm kin} = 35$ MeV, 3° (······) and 500 MeV, 0.21° (− · · · −), as well as the scaled DWi results at 35 MeV, 3° (———). The bottom curves (multiplied by a factor of 0.1 for better visibility) show the PM results (− · − · −) and the SM results (− − −−) as well as the scaled SM results at $E_{i,\rm kin} = 35$ MeV, 3° (······). The solid line is a copy of the scaled DWi results from the top. (c) $\frac{d^2\sigma}{d\omega d\Omega_k}$ at $E_{i,\rm kin} = 100$ MeV and $\theta_k = 3.5°$. The top curves show the PM results (− · −), and the scaled PM results at $E_{i,\rm kin} = 35$ MeV, 10° (······) and at 500 MeV, 0.7° (− · · · −), as well as the scaled DWi results at 35 MeV, 10° (———). The bottom curves (multiplied by a factor of 0.1) show the SM results (− − −−) and the scaled SM results at 35 MeV, 10° (······) and at 500 MeV, 0.7° (− · −). The solid line is a copy of the scaled DWi results from the top.

compared to those of the DW theory. For 35-MeV collisions, the deviation between these two theories is near $E_{f,\rm kin} = 5$ MeV, about 17%, slightly decreasing with E_f. By considering the scaled SM results at collision energies up to 500 MeV (scaling requires $\theta_k = 0.7°$ at 500 MeV), we conjecture that also for the DW theory the scaling will break down near $E_{f,\rm kin} = 3$ MeV. Although the PM results approach the SM ones with increasing impact energy, there remains an overestimate of the SM theory by the PM theory at 500 MeV of about 37% for $E_{f,\rm kin} \gtrsim 5$ MeV.

C. Singly differential cross section

Except for the Di Piazza–Milstein theory which cannot be used at small angles, the singly differential cross section for the photon spectrum is obtained from the numerical integration,

$$\frac{d\sigma}{d\omega} = 2\pi \int_0^\pi \sin\theta_k d\theta_k \frac{d^2\sigma}{d\omega d\Omega_k}, \tag{3.2}$$

with the doubly differential cross section from (2.1) for the SM theory, respectively, from (2.3) for the DSM, the DaSM, and the Dirac partial-wave theories.

Milstein and coworkers [24] employ a different approach for the calculation of the photon spectrum. It is based on the replacement of $\psi_f^{(\sigma_f)}\psi_f^{(\sigma_f)+}$, occurring in (2.1) with (2.2), when integrated over $d\Omega_f$ and summed over σ_f, by semiclassical Green's functions, derived in Ref. [25]. For the photon spectrum, independent of any angular variables, a similar replacement is possible for the initial states. In order to facilitate convergence, the first-order Born cross section is subtracted. Hence, only the Coulomb distortion corrections, considered up to first order in c^2/E_i, remain to be evaluated. Using that basically small angles contribute to the angle-integrated cross section, the result for a pure Coulomb field can be obtained analytically [24] as

$$\begin{aligned}\frac{d\sigma^{\rm Mil}}{d\omega} = \frac{d\sigma^{\rm PWBA}}{d\omega} - \frac{4}{\omega}\left(\frac{e^2}{c}\right)^3 \frac{Z^2}{c^4}\bigg\{\left[y^2 + \frac{4}{3}(1-y)\right] f_1 \\ - \frac{\pi^3(2-y)\,c^2}{8(1-y)\,E_i}\left[y^2 + \frac{3}{2}(1-y)\right] f_2\bigg\},\end{aligned} \tag{3.3}$$

with $y = \omega/E_i$, the Born cross section $\frac{d\sigma^{\rm PWBA}}{d\omega}$ obtained via (3.2) from the respective doubly differential cross section (see, e.g., Refs. [26,27]), and

$$\begin{aligned} f_1 &= {\rm Re}\{\psi(1 + iZ/c) + C\}, \\ f_2 &= \frac{Z}{c}{\rm Re}\left\{\frac{\Gamma(1 - iZ/c)\,\Gamma\left(\frac{1}{2} + iZ/c\right)}{\Gamma(1 + iZ/c)\,\Gamma\left(\frac{1}{2} - iZ/c\right)}\right\}, \end{aligned} \tag{3.4}$$

where $\psi(x) = \frac{d}{dx}\ln\Gamma(x)$, and $C = 0.577\,215\ldots$ is Euler's constant.

Figure 6(a) shows the photon spectrum at the collision energy of 35 MeV, calculated from the various theories. Clearly the Dirac partial-wave result, feasible only up to $E_{f,\rm kin} = 3$ MeV, approaches the SM estimates with increasing energy of the scattered electron. The Milstein theory, invalid near the SWL because of the factor $(1 - \omega/E_i)^{-1}$ in (3.3), coincides

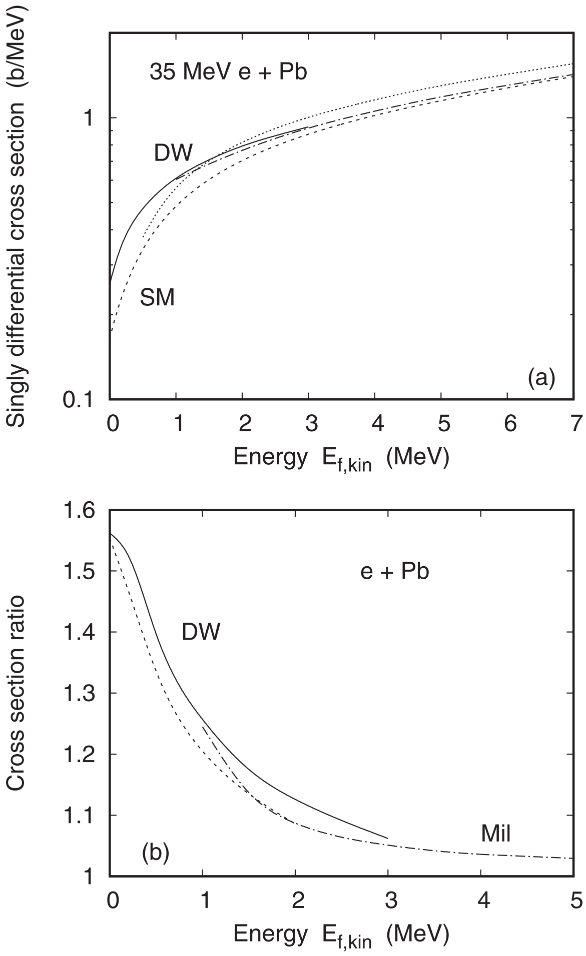

FIG. 6. (a) Singly differential bremsstrahlung cross section $\frac{d\sigma}{d\omega}$ from 35-MeV electrons colliding with ^{208}Pb as a function of final electron energy $E_{f,\mathrm{kin}}$. Shown are results from the interpolation of the DSM theory (at the SWL) and the merged DWm theory (for $E_{f,\mathrm{kin}} \geqslant 0.2$ MeV) (——), from the SM theory (− − −−), and from the Milstein theory (− · −). Included are results from the first-order Born approximation (· · · · · ·). (b) Cross-section ratio $\frac{d\sigma/d\omega}{d\sigma^{\mathrm{SM}}/d\omega}$ with respect to the SM result from the interpolation of the DSM and the DWm theory (——) and from the Milstein theory (− · −) at 35 MeV as a function of $E_{f,\mathrm{kin}}$. Included is the respective ratio from the interpolation of the DSM and the DaSM results at 100 MeV (− − −−, taken from Ref. [12]).

with the DW theory near $E_{f,\mathrm{kin}} = 3$ MeV and provides a nice approximation to the SM theory at energies exceeding 5 MeV. The first-order Born result is shown in addition to provide an estimate of the distortion effects for the Pb target.

In Fig. 6(b) the deviation of the DW and the Milstein theory from the SM model, expressed in terms of the cross section ratios, is displayed. The Milstein estimates, viewed as an extension of the DW results to higher E_f, support the validity of the Sommerfeld-Maue theory for the singly differential cross section at photon frequencies up to a distance of about 5 MeV from the tip of the spectrum (with deviations between the two theories of ≈2% at $E_{f,\mathrm{kin}} = 7$ MeV). Included in Fig. 6(b) is the ratio $d\sigma^{\mathrm{DaSM}}/d\sigma^{\mathrm{SM}}$ at 100-MeV impact, assuming the validity of the scaling rules. However, this ratio is slightly too small, because the DaSM results underestimate the DW ones at the higher angles which still contribute to the angle-integrated cross section.

TABLE I. Validity region of the Dirac partial-wave (DW), Dirac–Sommerfeld-Maue (DSM), asymptotic DSM (DaSM), Sommerfeld-Maue (SM), and Milstein (Mil) theories at collision energies $E_{i,\mathrm{kin}} \geqslant$ 35 MeV in terms of the final kinetic electron energy $E_{f,\mathrm{kin}}$ (respectively in terms of an interval of $E_{f,\mathrm{kin}}$).

Theory	$E_{i,\mathrm{kin}}$ (MeV)	$E_{f,\mathrm{kin}}$ (MeV)
DW	35	[0.2,3]
Scaled DW	>35	[0.2,3]
DSM	$\gtrsim$35	0
DaSM	$\gtrsim$35	[0,2]
SM	$\gtrsim$35	$\gtrsim$5
Mil	$\gtrsim$35	$\gtrsim$3

Table I gives an overview of the validity regime of the investigated theories for the angle-integrated singly differential bremsstrahlung cross section.

D. Polarization correlations

It is well known that the investigation of polarization variables provides a more stringent test of the theoretical models than intensity studies where it is summed, respectively averaged, over the polarization degrees of freedom. In the preceding investigations we have probed the Sommerfeld-Maue approximation by comparing the resulting photon intensity with the one obtained from the Dirac partial-wave theory or related models. In the following, the polarization transfer from the incoming electron to the photon is examined. Restricting ourselves to the emission of a circularly polarized photon from an electron characterized by the polarization vector $\boldsymbol{\zeta}_i = (\zeta_{ix}, \zeta_{iy}, \zeta_{iz})$, the bremsstrahlung intensity can be obtained from the following formula [23,28],

$$\frac{d^2\sigma^{\mathrm{pol}}}{d\omega d\Omega_k}(\boldsymbol{\zeta}_i, \xi_2) = \frac{1}{2}\left(\frac{d^2\sigma}{d\omega d\Omega_k}\right) \times [1 - C_{12}\,\zeta_{ix}\xi_2 - C_{20}\zeta_{iy} + C_{32}\,\zeta_{iz}\xi_2], \tag{3.5}$$

where $\xi_2 = +1$ for right-circularly and $\xi_2 = -1$ for left-circularly polarized photons. The parameters C_{12}, C_{20}, and C_{32}, which depend on the photon frequency and angle, describe the spin asymmetry and are termed polarization correlations. A sensitive parameter is C_{12}, which relates to the polarization transfer of an electron originally polarized transversely to the beam direction (but within the scattering plane spanned by $\boldsymbol{k}_i$ and $\boldsymbol{k}$). It can be calculated from the relative cross-section difference,

$$C_{12} = -\frac{d^2\sigma^{\mathrm{pol}}(\boldsymbol{\zeta}_i, 1) - d^2\sigma^{\mathrm{pol}}(\boldsymbol{\zeta}_i, -1)}{d^2\sigma^{\mathrm{pol}}(\boldsymbol{\zeta}_i, 1) + d^2\sigma^{\mathrm{pol}}(\boldsymbol{\zeta}_i, -1)}, \tag{3.6}$$

with $\boldsymbol{\zeta}_i = (1, 0, 0)$.

Figure 7 displays the angular dependence of C_{12} for a collision energy of 35 MeV and fixed final energies $E_{f,\mathrm{kin}}$ ranging from 1.5 to 11 MeV. For 11 MeV, convergence reasons prohibit the DW calculations below 4°. It is seen that even at a rather high final energy of 5 MeV, where the photon intensity obtained from the SM theory deviates by only 15–30% from

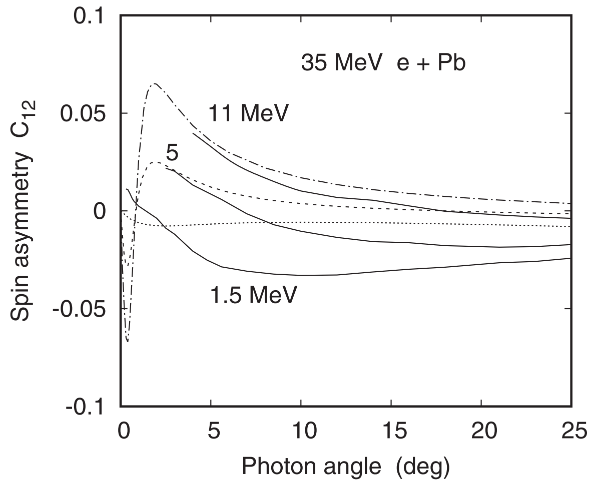

FIG. 7. Spin asymmetry C_{12} for circularly polarized bremsstrahlung from 35-MeV transversely polarized electrons colliding with ^{208}Pb as a function of the photon angle θ_k. Shown are DW results (———) at $E_{f,\mathrm{kin}} = 1.5$ MeV (lower curve), 5 MeV (middle curve), and 11 MeV (uppermost curve). Also shown are the SM results for 1.5 MeV (······), 5 MeV (− − −−), and 11 MeV (− · −).

the DW result at angles between 5° and 20° [see Fig. 1(b)], the spin asymmetry still differs strongly for the two models, even in sign. An agreement of the spin asymmetry estimates within the two theories is only expected well beyond $E_{f,\mathrm{kin}} =$ 10 MeV. In this context it should be noted that a correct prediction of C_{12} is only possible within the DW and the DSM theories. However, all models based on the approximate wave function (2.5) fail [12].

IV. CONCLUSION

We have provided bremsstrahlung estimates from five current prescriptions, the Dirac partial-wave theory, the Dirac asymptotic Sommerfeld-Maue theory, and the Sommerfeld-Maue approximation, as well as two approaches from Milstein and coworkers, an approximate DaSM model and a prescription for the singly differential cross-section based on semiclassical Green's functions. The DaSM results served basically as a complement to the DW results at very small photon angles, where a too large number of partial waves would be needed. At the tip of the photon spectrum, the more accurate DSM results were used instead.

The applicability of the SM approximation was investigated by means of a comparison with the state-of-the-art DW theory, evaluated at 35 MeV, which is the highest collision energy for which DW calculations are feasible. The heavy lead target was chosen to probe the SM functions beyond their semirelativistic range of validity. It turned out that the smaller the photon angle the larger is the photon frequency up to which the SM model provides reliable results. Near zero degrees the SM estimates are reasonable up to about 3 MeV below the tip, whereas at 10° the difference between the DW and the SM results for even 11 MeV below the tip is still about 15%, increasing to nearly 30% at 20°. The Di Piazza-Milstein approximation for the doubly differential cross section overpredicts in general the DW estimates, the more so, the smaller the photon angle. However at large angles and not too high final electron energies, the PM results for the angular dependence are close to the ones predicted by the SM model.

We have also investigated the validity of a high-energy small-angle scaling law, which predicts a linear increase of the doubly differential cross section with collision energy if the photon angle is decreased by the same amount. It turned out that this scaling holds already at impact energies as low as 35 MeV near the tip for those angles contributing predominantly to the singly differential cross section. At the larger photon angles the scaling is no longer strictly verified; however, it improves with collision energy. The scaling also loses its validity further off the tip. This results from the fact that the smallness of E_f/E_i and of c^2/E_i enter into the derivation of the scaling law [12]. Hence, at final kinetic electron energies as high as 10 MeV, a minimum collision energy of at least 100 MeV is required for the scaling to hold, as conjectured from the SM and PM results.

Concerning the singly differential cross section for the photon spectrum, the scaling property can be used for providing DW estimates at impact energies beyond 35 MeV, if the final electron energy does not exceed 3 MeV. The validation of this property is based on the scaling results of the DSM, DaSM, and SM theories, their evaluation not being hampered by any restriction on the collision energy. The Milstein analytical Coulomb distortion correction, added to the first-order Born approximation, can be viewed as a complement to the DW theory at final kinetic energies beyond 3 MeV, where the results of these two theories become close to each other. The Milstein results are thereupon used to establish the validity of the SM approximation for the singly differential cross section beyond final kinetic electron energies around 5 MeV, where the difference between the two theories has decreased to 3%. In this context it should be noted that the Milstein prescription has already been tested successfully against the SM theory and experiment at the lower half of the photon spectrum [3].

A crucial validity test of the Sommerfeld-Maue theory requires, in addition to the photon intensity, the consideration of the polarization variables. Hereby, it turned out that at final energies where the photon intensity is already reasonably well reproduced by the SM theory, there remain serious discrepancies in the spin asymmetry. The present results lead to the conclusion that a final energy exceeding by far 10 MeV is required for a correct account of the polarization parameters within the SM theory. This is in accord with the early estimates by Bethe and Maximon [10] that an energy of the order of 50 MeV is needed for both the incoming electron and the scattered electron.

ACKNOWLEDGMENTS

I would like to thank A. I. Milstein and P. A. Krachkov for directing my interest to their work. It is a pleasure to thank A. Mangiarotti for stimulating this project and for calculating the Milstein Coulomb distortion corrections.

APPENDIX: THE Di PIAZZA-MILSTEIN CROSS SECTION FORMULA

In the Di Piazza–Milstein approach [14], the bremsstrahlung doubly differential cross section is given by

$$\frac{d^2\sigma^{\mathrm{PM}}}{d\omega d\Omega_k} = \frac{\omega k_f E_i E_f}{4\pi\, c^5\, k_i} \sum_{\kappa_f} \sum_{m_f=\pm\frac{1}{2}} [|G_{\kappa_f m_f}|^2 + |F_{\kappa_f m_f}|^2 + 4m_f \,\mathrm{Im}\,(F^*_{\kappa_f m_f} G_{\kappa_f m_f})], \tag{A1}$$

with

$$G_{\kappa_f m_f} = C_0 \left(l_f 0 \,\frac{1}{2}\, m_f |\, j_f m_f \right)(-i) \times \sqrt{\frac{E_f + c^2}{E_f}}(2k_f)^{\gamma-1}[e^{i\xi} I_{R_1} - e^{-i\xi} I_{R_2}] \tag{A2}$$

and

$$F_{\kappa_f m_f} = C_0 \left(l'_f 0 \,\frac{1}{2}\, m_f |\, j_f m_f \right) \times \sqrt{\frac{E_f - c^2}{E_f}}(2k_f)^{\gamma-1}[e^{i\xi} I_{R_1} + e^{-i\xi} I_{R_2}]. \tag{A3}$$

The normalization constant C_0 is

$$C_0 = \frac{2}{(k\sin\theta_k)^2}\left(\frac{2k_i}{k^2\sin^2\theta_k}\right)^{-i\eta_i} \frac{\Gamma(1-i\eta_i)}{\Gamma(i\eta_i)} \times \sqrt{2l_f+1}\, e^{\pi\eta_f/2}\, \frac{|\Gamma(\gamma+1+i\eta_f)|}{\Gamma(2\gamma+1)}, \tag{A4}$$

where $\gamma = \sqrt{\kappa_f^2 - (Z/c)^2}$, $\eta_f = \frac{ZE_f}{k_f c^2}$, and $e^{-2i\xi} = \frac{\gamma - i\eta_f}{\kappa_f - i\eta_f c^2/E_f}$. The radial integrals are denoted by I_{R_1} and I_{R_2}. Their analytical values are

$$I_{R_1} = C_1\, {}_2F_1\left(\gamma - i\eta_f, \gamma + i\eta_i, 2\gamma+1, \frac{2k_f}{k_f + E_f/c}\right),$$
$$I_{R_2} = C_1\, {}_2F_1\left(\gamma + 1 - i\eta_f, \gamma + i\eta_i, 2\gamma+1, \frac{2k_f}{k_f + E_f/c}\right),$$
$$C_1 = \Gamma(\gamma + i\eta_i)[\epsilon - i(E_f/c + k_f)]^{-(\gamma+i\eta_i)}, \tag{A5}$$

where ${}_2F_1$ is a hypergeometric function and $\epsilon \to 0$.

[1] J. A. García-Alvarez *et al.*, J. Phys. B **50**, 155003 (2017).
[2] J. A. García-Alvarez, J. M. Fernández-Varea, V. R. Vanin, and N. L. Maidana, J. Phys. B **51**, 225003 (2018).
[3] A. Mangiarotti *et al.*, Phys. Lett. B **815**, 136113 (2021).
[4] A. Mangiarotti and M. N. Martins, Radiat. Phys. Chem. **141**, 312 (2017).
[5] A. Poškus, At. Data Nucl. Data Tables **129-130**, 101277 (2019).
[6] R. H. Pratt, R. A. Müller, and A. Surzhykov, Phys. Rev. A **93**, 053421 (2016).
[7] D. H. Jakubassa-Amundsen, Radiat. Phys. Chem. **162**, 172 (2019).
[8] H. K. Tseng and R. H. Pratt, Phys. Rev. A **3**, 100 (1971).
[9] V. A. Yerokhin and A. Surzhykov, Phys. Rev. A **82**, 062702 (2010).
[10] H. A. Bethe and L. C. Maximon, Phys. Rev. **93**, 768 (1954).
[11] D. H. Jakubassa-Amundsen, Phys. Rev. A **82**, 042714 (2010).
[12] D. H. Jakubassa-Amundsen, J. Phys. G: Nucl. Part. Phys. **47**, 075102 (2020).
[13] R. J. Jabbur and R. H. Pratt, Phys. Rev. **129**, 184 (1963).
[14] A. Di Piazza and A. I. Milstein, Phys. Rev. A **85**, 042107 (2012).
[15] G. Elwert and E. Haug, Phys. Rev. **183**, 90 (1969).
[16] R. J. Jabbur and R. H. Pratt, Phys. Rev. **133**, B1090 (1964).
[17] A. R. Edmonds, *Angular Momentum in Quantum Mechanics*, 2nd ed. (Princeton University, Princeton, NJ, 1960).
[18] H. Brysk, C. D. Zerby, and S. K. Penny, Phys. Rev. **180**, 104 (1969).
[19] R. H. Pratt, Phys. Rev. **117**, 1017 (1960).
[20] F. Salvat, J. M. Fernández-Varea, and W. Williamson, Jr., Comput. Phys. Commun. **90**, 151 (1995).
[21] H. De Vries, C. W. De Jager, and C. De Vries, At. Data Nucl. Data Tables **36**, 495 (1987).
[22] R. H. Pratt and I. J. Feng, in *Atomic Inner Shell Physics*, edited by B. Crasemann (Plenum, New York, 1985).
[23] D. H. Jakubassa-Amundsen, Phys. Rev. A **93**, 052716 (2016).
[24] R. N. Lee, A. I. Milstein, V. M. Strakhovenko, and O. Ya. Schwarz, J. Exp. Theor. Phys. **100**, 1 (2005).
[25] R. N. Lee, A. I. Milstein, and V. M. Strakhovenko, J. Exp. Theor. Phys. **90**, 66 (2000).
[26] E. Borie, Nuovo Cimento A **11**, 969 (1972).
[27] V. B. Berestetskii, E. M. Lifshitz, and L. P. Pitaevskii, *Quantum Electrodynamics*, Course of Theoretical Physics Vol. 4, 2nd ed. (Elsevier, Oxford, 1982), p. 402.
[28] H. K. Tseng and R. H. Pratt, Phys. Rev. A **7**, 1502 (1973).